Hot-Dip Galvanizing of Functional Structural Steels

KUO-MIN HSU, KAI-CHENG CHANG, and CHAO-SUNG LIN
Department of Materials Science and Engineering

Abstract

Hot-dip galvanized coatings provide both barrier and sacrificial protection over steels and have found extensive applications. This study investigated the hot-dip galvanizing behavior of functional structural steels, including high-strength SBHS500, SM570M steels, and SN490B, SN490C structural steels, with emphasis on the microstructure, mechanical properties, and corrosion resistance of the hot-dip galvanized steels. It was found that hot-dip galvanizing treatment hardly affected the mechanical properties of the steel substrates. The coating was mainly composed of ζ and η phases regardless of the composition of the steel substrate. However, the morphology and distribution of the ζ phase was different on the distinct steels. Finally, δ phase was observed at the coating/steel interface with a characteristic dissolved morphology on SBHS500 and SM570M steels.

1. Introduction

In recent decades, steels have become principal materials for constructions such as bridges and buildings owing to the properties of high strength, light weight, good workability, and short construction period, and recyclability compared with those made of reinforced concrete. Corrosion on steels is, however, a critical issue of concern to many researchers and engineers especially in rainy and humid Taiwan. Serious corrosion can cause unexpected formation of cracks or oxides on the surface, which lowers the strength of the material. Corrosion prevention is, therefore, necessary for steels of constructions. Hot-dip galvanization (HDG) is one promising anti-corrosion method and possesses the advantage of averagely low annual cost and good durability [1-5]. Steels can thus be protected efficiently in corrosive environments by giving sacrificial anode protection through HDG process.

Different types of steels can be employed in different situations. Taiwan is located between Eurasian plates, resulting in frequently earthquake occurring, which makes that anti-seismic property is definitely one factor needed considering. As a result, it draws our attention to the properties of welded structural steels after HDG. Bergengren and Melander [6] reported that the fatigue limit of HDG high strength steels was reduced compared to uncoated counterparts. For the impact of welding processes on the properties, several literature were investigated as well [7,8]. However, the study of the influence of HDG process on the corrosion behavior and

mechanical properties of welded steels is still lacking.

In this research, steels for bridge high performance structures (SBHS) 500 and hot rolled anti-seismic steel SM570M, refractory steel SN490B, and SN490C were investigated. The results were divided into two segments. One is the microstructure and phases of steels above the substrate after HDG. Second is the influence of HDG process on the tensile strength of different welded steels.

2. Experimental method

2.1 Samples preparation

Four types of HDG steels, including SBHS 500, hot rolled SM570M, SN490B, and SN490C, received from Taiwan Galvanizing co., ltd. were investigated. The chemical compositions and mechanical properties are listed in Table 1. Every specimen was hot mounted in bakelite powders before grinding and testing. The hot mounted specimen was ground from 80 grit to 2500 grit SiC paper, followed by final polishing with diamond paste of 0.5 μm in the particle size. The welded steels with HDG coatings were prepared in the same way.

Steels	Chemical composition (wt%)					Yield strength (N/mm^2)	Tensile strength (N/mm^2)
	C	Si	Mn	P	S		
SN490B	≤0.18	≤0.55	≤1.60	≤0.03	≤0.015	≥325	490~610
SN490C	≤0.18	≤0.55	≤1.6	≤0.02	≤0.008	350~550	650~880
SBHS500	≤0.11	≤0.55	≤2.0	≤0.02	≤0.006	≥500	570~720
SM570MB	≤0.18	≤0.55	≤1.6	≤0.02	≤0.008	420~540	570~720

Table 1 Chemical compositions, yield strength, and tensile strength of SN490B, SN490C, SBHS500, and SM570MB.

2.2 Structure and phase analysis

The metallographic structure of cross section of the HDG steel specimen was observed using optical microscopy (OM) and scanning electron microscopy (SEM). To identify the phase in the coating after HDG, Fe-Zn phase diagram [9] was consulted and chemical stripping was employed. Chemical stripping was conducted by immersing the specimen in the solution of 7.5 vol% HCl, along with recording the open circuit potential (OCP). Four stages could be distinguished in each type of steel. Each specimen was rinsed with deionized water and subsequently dried with cooling

air as soon as it stopped the immersing test. The morphology of tested specimen in each selected time (in each stage) were identified using SEM and x-ray diffractometer (XRD).

2.3 Tensile test of welded steels

Flux cored arc welding (FCAW) was employed to conduct the welding on the steels. To quantitatively discuss the mechanical property of welded steel after HDG process, tensile test was employed by following the ASTM E8 standard. Four welded steels after HDG process were conducted at 20 mm / min in the tensile test and they were compared with that itself prior to the HDG.

3. Results and discussion

3.1 Metallographic cross section

Fig. 1 shows the cross section of the four types of steels after HDG. The phase boundary can be identified by chemical etching due to the different etching rates of the distinct phases. The thickness of coating in each steel lies between 200 and 250 μm. From the finely broken contrast distribution, it is reasonable to obtain the result that the other phase in the coating grew continuously instead of growing layer by layer. Images with higher magnification of cross sections are shown in Fig. 2. The SEM images, along with the EDS analysis, demonstrate that dark contrasts represent Zn-rich phase with approximate 7 at% in Fe content and bright contrasts represent pure zinc as marked with ζ and Zn, respectively.

3.2 Coating analysis

The state of the surface in 7.5 vol% HCl was investigated by recording OCP as shown in Fig. 3. From the chemical stripping in these plots, one identical trend is that they are able to be divided into four stages, which are marked as I, II, III, and IV, respectively. The surface microstructure of different time as marked with star, indicating four stages, were observed under SEM. Owing to the similar behavior of each steel, the morphology in 25 s, 75 s, 350 s, and 650 s of SBHS500, taken as representative, were observed under SEM, as demonstrated in Fig. 4. In stage I, the morphology is granular with the same order in the particle size. In stage II, all the granular particles turn to the rod-shape microstructure. When the immersion time was increased to 350s at stage III, column-shaped microstructure dominates the morphology. In the final stage, all the characteristic microstructure disappears and a plain surface shows up.

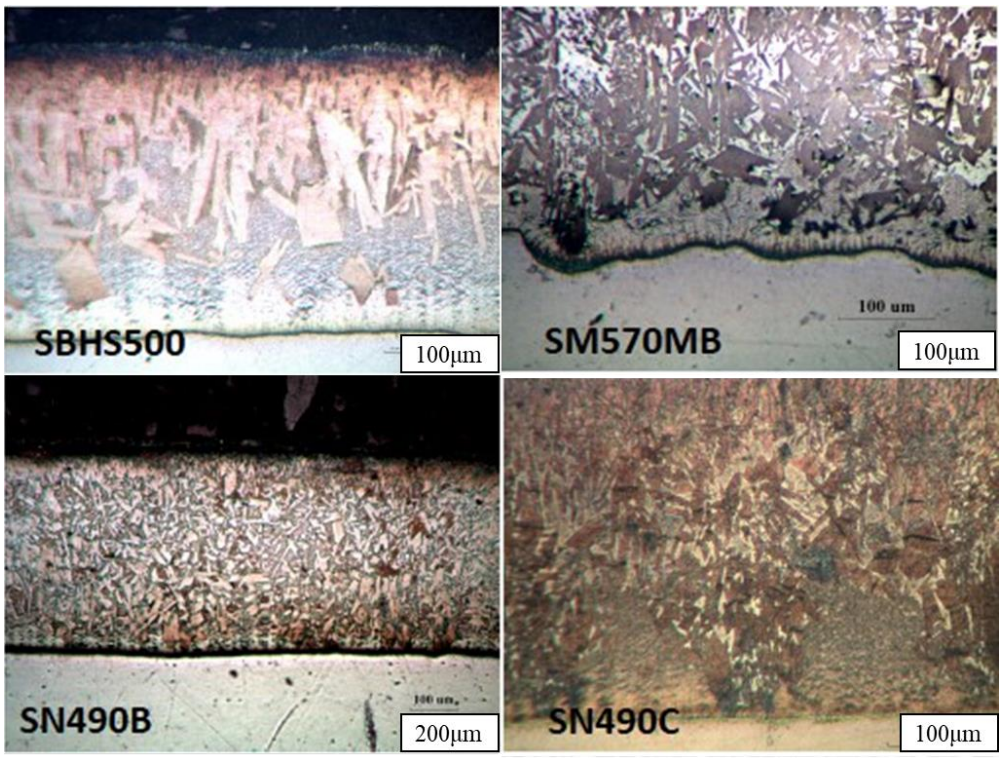

Fig. 1. Cross sections of SN490B, SN490C, SBHS500, and SM570MB under OM.

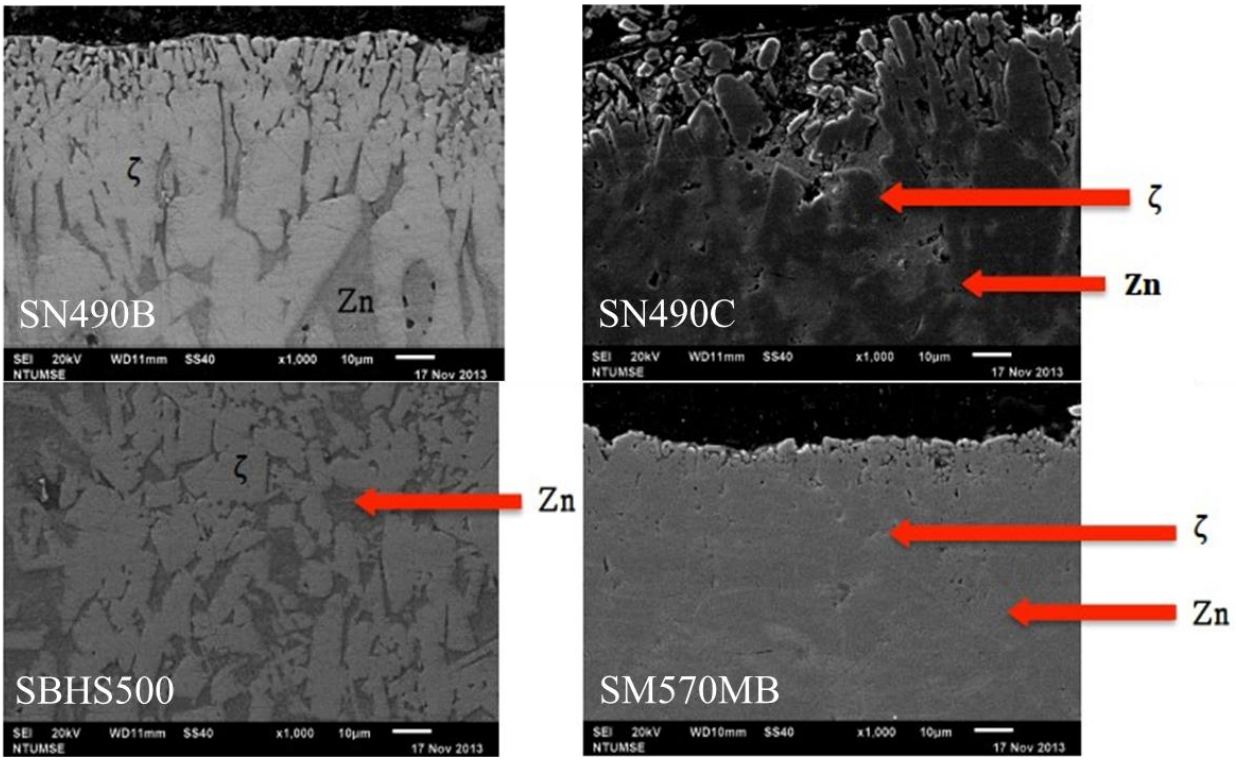

Fig. 2. Cross sections of SN490B, SN490C, SBHS500, and SM570MB under SEM.

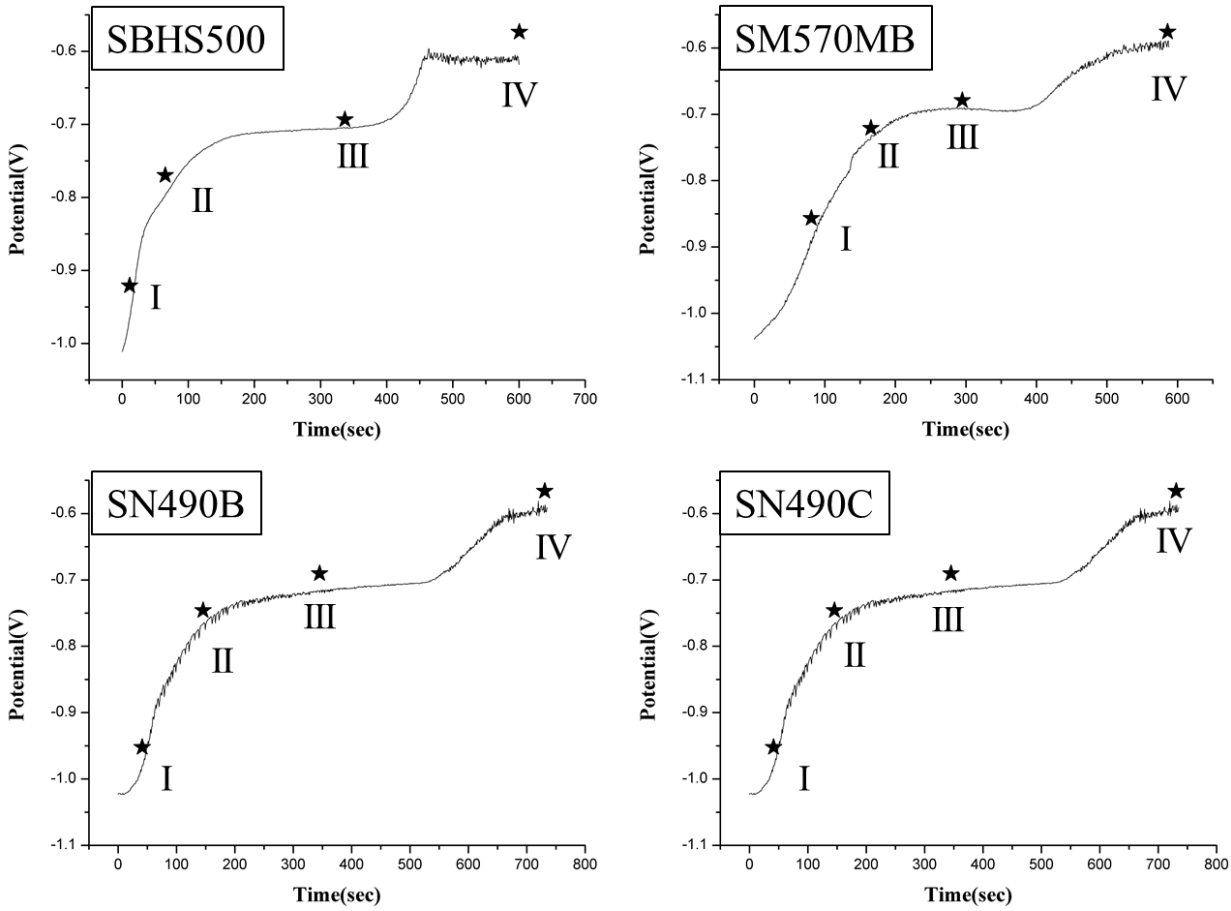

Fig. 3. OCP of SN490B, SN490C, SBHS500, and SM570MB in 7.5vol% HCl.

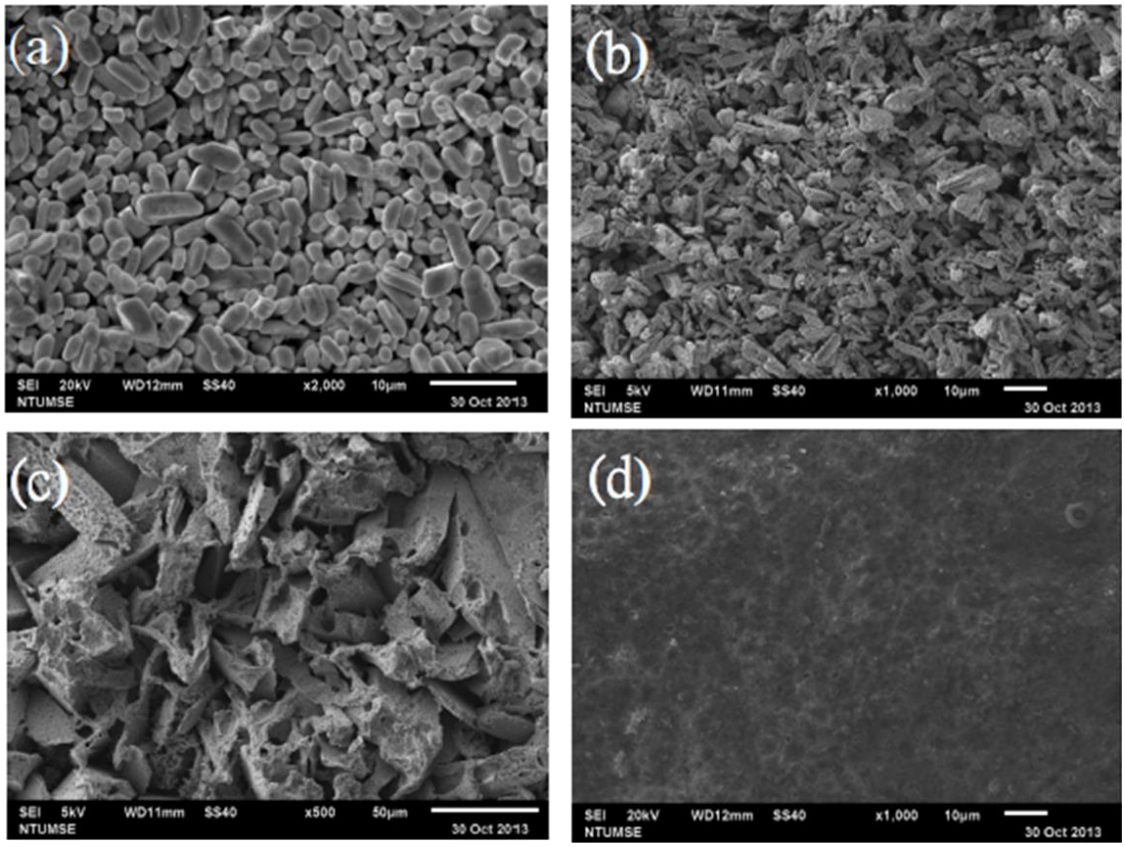

Fig. 4. Morphology in (a) 25s, (b) 75s, (c) 350s, and (d) 650s of SBHS500.

To identify the phases in each stage, XRD was used and the results are demonstrated in Fig. 5. The XRD patterns show that the principal phases are ζ and Zn, which corresponds to the results shown in Fig. 2. This is consistent with the results made by Belin et al. [10]. From the start of the chemical stripping to stage III appearing at approximately 350 s, only ζ and Zn exist in the coating. At stage IV, the Fe phase did not show up until the solution reached the substrate.

3.3 Welded steels after HDG

Fig. 6 shows the cross sections of HDG welded SBHS500 in distinct regions, including welding zone, heat affected zone (HAZ), and base metal zone. The base metal zone is in the same microstructure as that observed in Fig. 1 while the particle size of Fe-Zn phase in HAZ is much smaller. In addition, the thickness of coating in the welding zone is approximately 300 μm and this zone has the smallest particle size of Fe-Zn phase among the three regions.

The comparison of tensile strength of every welded steel before and after HDG is shown in Fig. 7(a). The results show that there is no evident change in tensile strength after the HDG process, indicating that HDG does not have negative impact on the tensile behavior. Fig. 7(b) displays that the failure interfaces of SBHS500 before and after HDG process belong to ductile fracture and other welded steels have the same behavior. Moreover, the fracture position of each welded steel is situated in the base metal instead of the welding zone, implying the enough high strength in this region.

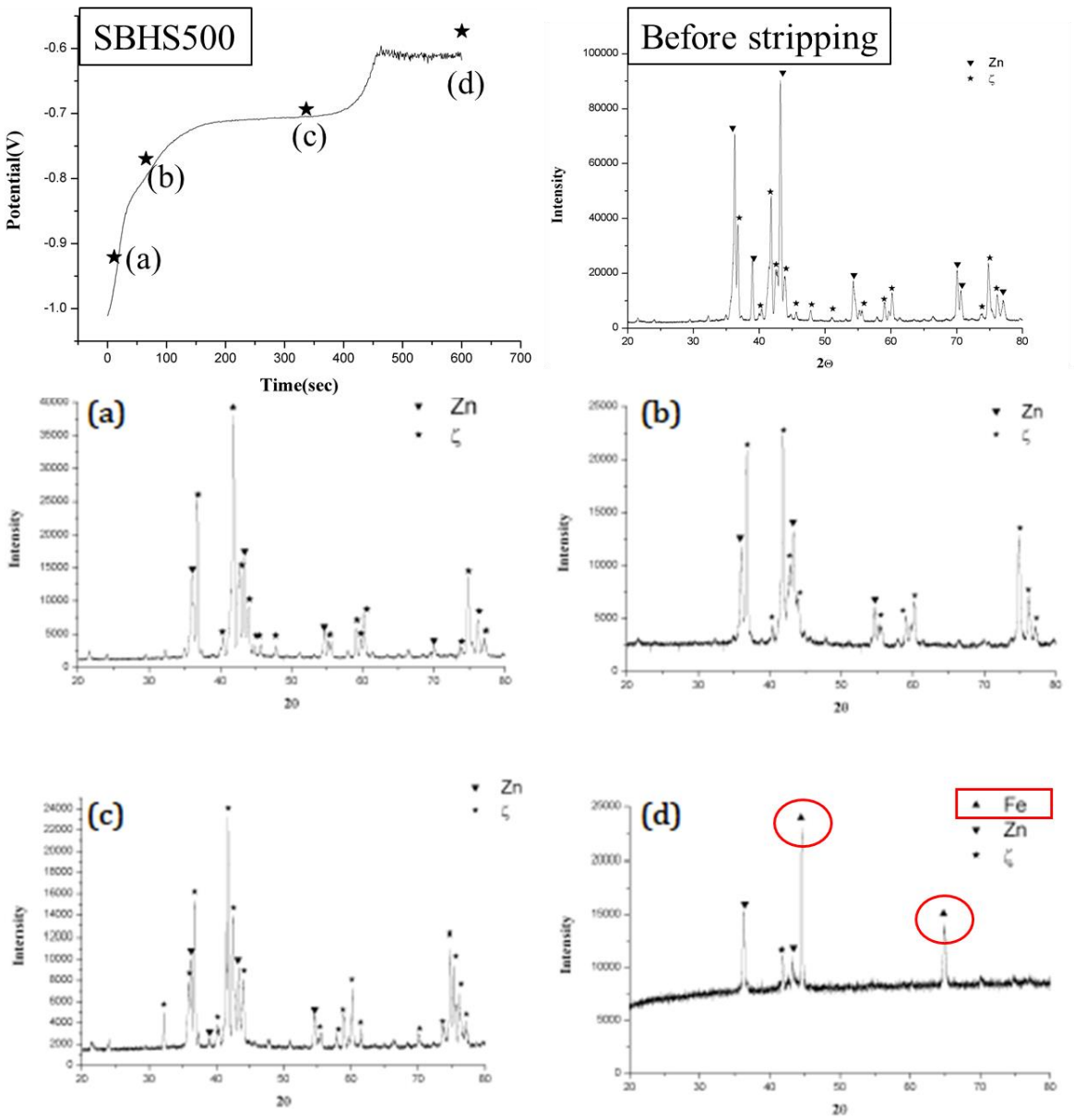

Fig. 5. XRD pattern prior to the chemical stripping of SBHS500, and the patterns from the start of the test at (a) 25 s, (b) 75 s, (c) 350 s, and (d) 650 s.

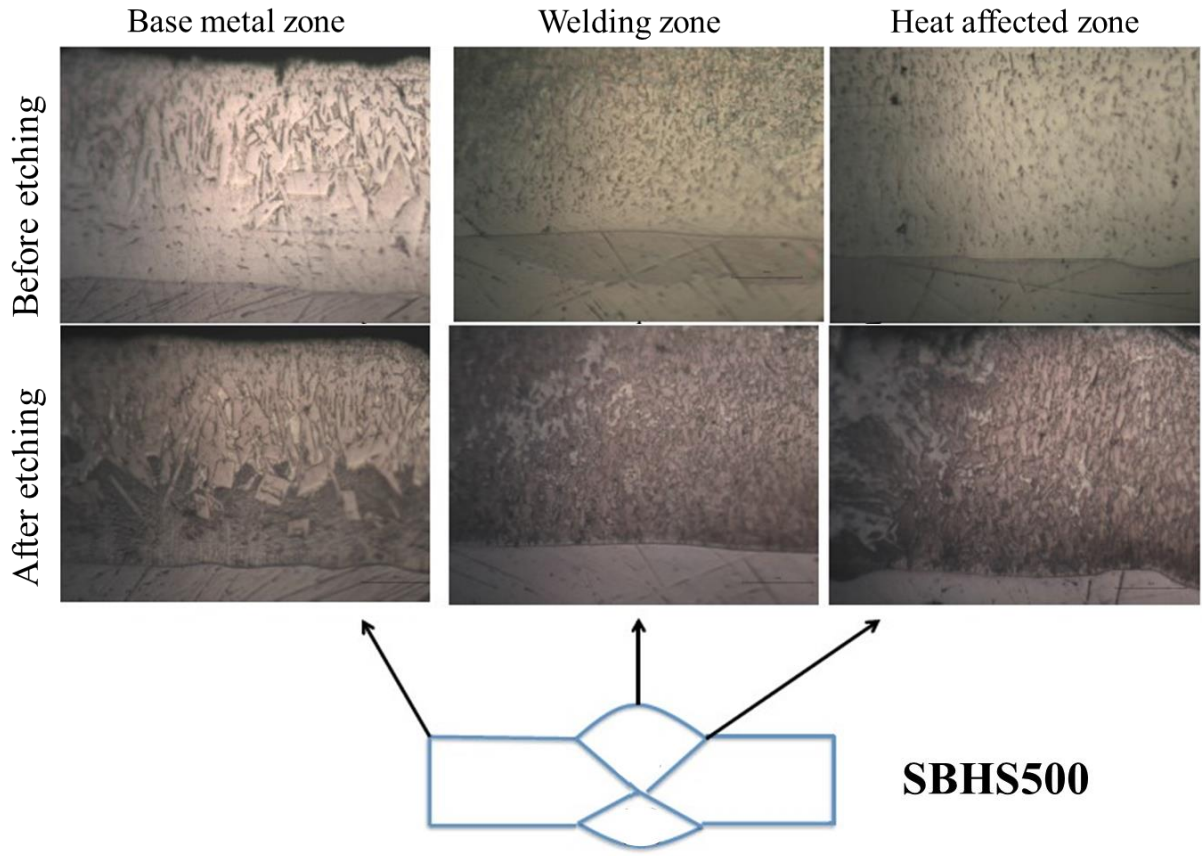

Fig. 6. Cross section of welded SBHS500 after HDG process before etching and after etching under OM.

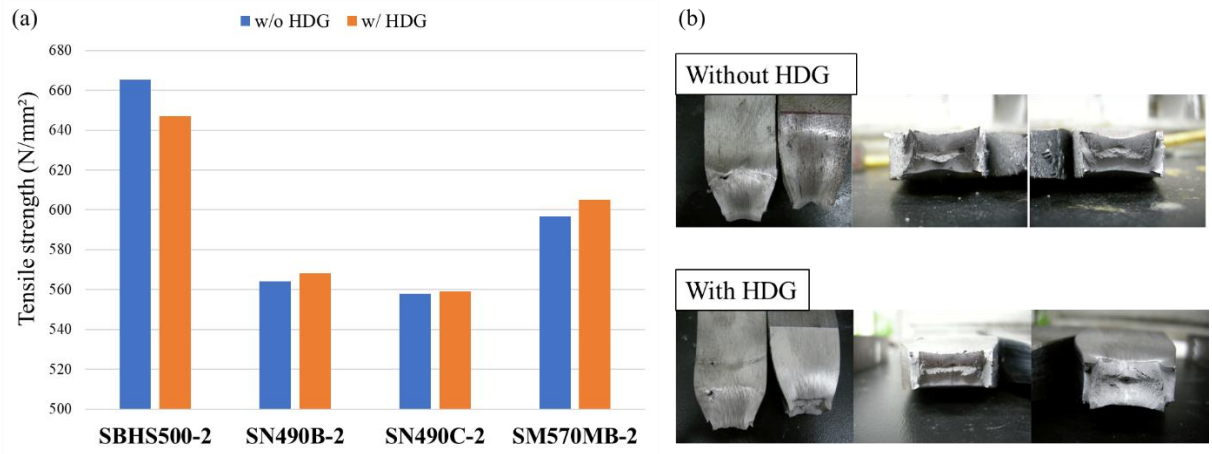

Fig. 7. (a) Tensile strength of different welded steels and (b) failure interface of SBHS500 with and without HDG.

4. Conclusions

Microstructure of the HDG steels:

1) The Fe-Zn intermetallic phases present in the HDG coating was stripped using

chemical stripping and identified with XRD and SEM, along with OCP recorded.
2) A lot of small and non-compact granular Fe-Zn compounds, identified as ζ phase, formed in the HDG coating, presumably due to the lack of Fe-Al barrier (low Al content).

Mechanical properties of the HDG steels and HDG welded steels:
1) There is no evident change in tensile strength of every welded steel after HDG.
2) Both the fracture interfaces before and after HDG belong to ductile fracture and all the fracture positions are situated in the matrix material.
The mechanical properties demonstrate that the HDG process has negligible impact on the mechanical properties of the welded SN490B, SN490C, SBHS500, and SM570MB.

Acknowledgement
This study was financially supported by the Galvanizing Association of Twain.

References

[1] R. Baboian, Corrosion Tests and Standards: Application and Interpretation, ASTM, Philadelphia (1995) 513.
[2] A.R. Marder. The metallurgy of zinc-coated steel. Progress in Materials Science 45 (2000) 191-271.
[3] M. Gavrila, J.P. Millet, H. Mazille, D. Marchandise, J.M. Cuntz. Corrosion behaviour of zinc–nickel coatings, electrodeposited on steel. Surface and Coatings Technology 123 (2000) 164-172.
[4] K. R. BALDWIN, M. J. ROBINSON, and C. J. E. SMITH. THE CORROSION RESISTANCE OF ELECTRODEPOSITED ZINC-NICKEL ALLOY COATINGS. Corrosion Science 35 (1993) 1267-1272.
[5] S.M.A. Shibli, B.N.Meena, R. Remya. A review on recent approaches in the field of hot dip zinc galvanizing process. Surface & Coatings Technology 262 (2015) 210-215.
[6] Yngve Bergengren and Arne Melander. An experimental and theoretical study of the fatigue properties of hot dip-galvanized high-strength sheet steel. Int J Fatigue 14 (1992) 154-162.
[7] R. Nandan, T. DebRoy, H.K.D.H. Bhadeshia. Recent advances in friction-stir welding - Process, weldment structure and properties. Progress in Materials Science 53 (2008) 980-1023.
[8] E.O. Olakanmi, R.F. Cochrane, K.W. Dalgarno. A review on selective laser sintering/melting (SLS/SLM) of aluminium alloy powders: Processing,

microstructure, and properties. Progress in Materials Science 74 (2015) 401-477.
[9] Okamoto, H. Fe-Zn (Iron-Zinc). J. Phase Equilibr. Diff. 28 (2007) 317-318.
[10] Claude H. E. Belin and Renaud C. H. Belin. Synthesis and Crystal Structure Determinations in the C and d Phase Domains of the Iron-Zinc System: Electronic and Bonding Analysis of Fe13Zn39 and FeZn10, a Subtle Deviation from the Hume-Rothery Standard?. Journal of Solid State Chemistry 151 (2000) 85-95.